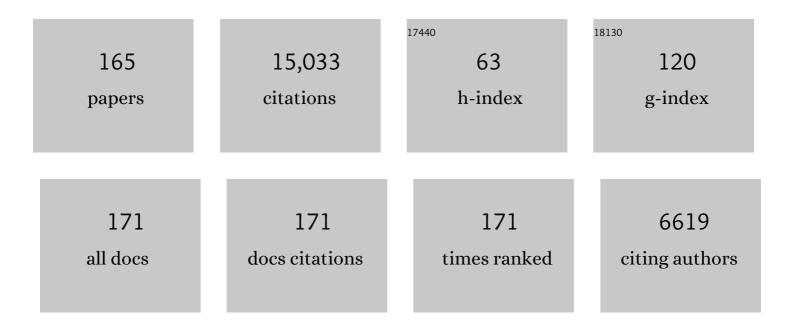
Leonid V Danyushevsky

List of Publications by Year in descending order

Source: https://exaly.com/author-pdf/9120586/publications.pdf Version: 2024-02-01



#	Article	lF	CITATIONS
1	Use of Nonâ€Matrix Matched Reference Materials for the Accurate Analysis of Calcium Carbonate by LAâ€ICPâ€MS. Geostandards and Geoanalytical Research, 2022, 46, 97-115.	3.1	5
2	Sedimentary pyrite proxy for atmospheric oxygen: evaluation of strengths and limitations. Earth-Science Reviews, 2022, 227, 103941.	9.1	7
3	Implications of high-Mg# adakitic magmatism at Hunter Ridge for arc magmatism of the Fiji - Vanuatu region. Earth and Planetary Science Letters, 2022, 590, 117592.	4.4	1
4	Structural setting, wall rock alteration and gold mineralisation of the Mt. Percy gold deposit, Kalgoorlie, Western Australia. Mineralium Deposita, 2021, 56, 1449-1470.	4.1	4
5	Pyrite trace element behavior in magmatic-hydrothermal environments: An LA-ICPMS imaging study. Ore Geology Reviews, 2021, 128, 103878.	2.7	51
6	Assessment of the mineral ilmenite for U–Pb dating by LA-ICP-MS. Journal of Analytical Atomic Spectrometry, 2021, 36, 1244-1260.	3.0	9
7	Elimination of aliasing in LA-ICP-MS by alignment of laser and mass spectrometer. Journal of Analytical Atomic Spectrometry, 2021, 36, 733-739.	3.0	11
8	Laser ablation-ICPMS analysis of trace elements in pyrite from the Tharsis massive sulphide deposit, Iberian Pyrite Belt (Spain). Journal of Iberian Geology, 2021, 47, 429-440.	1.3	3
9	LA-ICP-MS analyses of trace elements in base metal sulfides from carbonate-hosted Zn-Pb deposits, South China: A case study of the Maoping deposit. Ore Geology Reviews, 2021, 130, 103945.	2.7	43
10	Pyroxenites from mantle section of Voykar Ophiolite – Melt/peridotite reaction and crystallization in SSZ mantle. Lithos, 2021, 388-389, 106063.	1.4	5
11	Revealing the multi-stage ore-forming history of a mineral deposit using pyrite geochemistry and machine learning-based data interpretation. Ore Geology Reviews, 2021, 133, 104079.	2.7	22
12	The origin of the Late Quaternary back-arc volcanic rocks from Kamchatka: evidence from the compositions of olivine and olivine-hosted melt inclusions. Contributions To Mineralogy and Petrology, 2021, 176, 1.	3.1	2
13	LA-ICP-MS sphalerite and galena trace element chemistry and mineralization-style fingerprinting for carbonate-hosted Pb-Zn deposits: Perspective from early Devonian Huodehong deposit in Yunnan, South China. Ore Geology Reviews, 2021, 136, 104253.	2.7	24
14	Phase relations of arsenian pyrite and arsenopyrite. Ore Geology Reviews, 2021, 136, 104285.	2.7	9
15	Protracted lifespan of the late Mesozoic multistage Qianlishan granite complex, Nanling Range, SE China: Implications for its genetic relationship with mineralization in the Dongpo ore field. Ore Geology Reviews, 2021, 139, 104445.	2.7	5
16	Recent advances in the application of mineral chemistry to exploration for porphyry copper–gold–molybdenum deposits: detecting the geochemical fingerprints and footprints of hypogene mineralization and alteration. Geochemistry: Exploration, Environment, Analysis, 2020, 20,	0.9	24
17	176-188. SW Pacific arc and backarc lavas and the role of slab-bend serpentinites in the global halogen cycle. Earth and Planetary Science Letters, 2020, 530, 115921.	4.4	22
18	Trace elements in sulfides from the Maozu Pb-Zn deposit, Yunnan Province, China: Implications for trace-element incorporation mechanisms and ore genesis. American Mineralogist, 2020, 105, 1734-1751.	1.9	33

LEONID V DANYUSHEVSKY

#	Article	IF	CITATIONS
19	Temporal and spatial evolution of the Neogene age Breiðdalur central volcano through 39Ar/40Ar and U-Pb age determination. Journal of Volcanology and Geothermal Research, 2020, 404, 107006.	2.1	2
20	Behavior of Trace Elements during Oxidation of Sphalerite of the Irinovskoe Hydrothermal Sulfide Field (13°20′ N, Mid-Atlantic Ridge). Geology of Ore Deposits, 2020, 62, 254-259.	0.7	3
21	Time-of-flight ICP-MS laser ablation zircon geochronology: assessment and comparison against quadrupole ICP-MS. Journal of Analytical Atomic Spectrometry, 2020, 35, 2282-2297.	3.0	6
22	Trace Element Geochemistry of Sulfides from the Ashadze-2 Hydrothermal Field (12°58′ N, Mid-Atlantic) Tj 2020, 10, 743.	ETQq0 0 0 2.0) rgBT /Overloc 10
23	Deconvolution of the composition of fine-grained pyrite in sedimentary matrix by regression of time-resolved LA-ICP-MS data. American Mineralogist, 2020, 105, 820-832.	1.9	16
24	Metallogenic model of the Jinchang Au-Ni deposit in the Ailaoshan belt, SW China, determined on the basis of pyrite trace element contents, in-situ sulfur isotope composition and PGE geochemistry. Ore Geology Reviews, 2020, 120, 103415.	2.7	4
25	Evidence for elevated and variable atmospheric oxygen in the Precambrian. Precambrian Research, 2020, 343, 105722.	2.7	30
26	Using Mineral Chemistry to Aid Exploration: A Case Study from the Resolution Porphyry Cu-Mo Deposit, Arizona. Economic Geology, 2020, 115, 813-840.	3.8	48
27	The effects of H2O, He, N2 and H2 on ion kinetic energies in inductively coupled plasma mass spectrometry. Spectrochimica Acta, Part B: Atomic Spectroscopy, 2020, 169, 105870.	2.9	10
28	Petrology, Geochemistry, and the Origin of Sulfide-Bearing and PGe-mineralized Troctolites from the Konnikov Zone in the Yoko-Dovyren Layered Intrusion. Russian Geology and Geophysics, 2020, 61, 611-633.	0.7	8
29	Timing of multiple magma events and duration of the hydrothermal system at the Yu'erya gold deposit, eastern Hebei Province, China: Constraints from U–Pb and Ar–Ar dating. Ore Geology Reviews, 2020, 127, 103804.	2.7	6
30	Distribution and occurrence of Ge and related trace elements in sphalerite from the Lehong carbonate-hosted Zn-Pb deposit, northeastern Yunnan, China: Insights from SEM and LA-ICP-MS studies. Ore Geology Reviews, 2019, 115, 103175.	2.7	43
31	Tellurium-Bearing Mineralization in Clastic Ores at the Yubileynoe Copper Massive Sulfide Deposit (Southern Urals). Geology of Ore Deposits, 2019, 61, 133-161.	0.7	5
32	The formation mechanisms of sedimentary pyrite nodules determined by trace element and sulfur isotope microanalysis. Geochimica Et Cosmochimica Acta, 2019, 259, 53-68.	3.9	53
33	New Olivine Reference Material for <i>In Situ</i> Microanalysis. Geostandards and Geoanalytical Research, 2019, 43, 453-473.	3.1	77
34	Trace Element Mapping of Copper- and Zinc-Rich Black Smoker Chimneys from Brothers Volcano, Kermadec Arc, Using Synchrotron Radiation XFM and LA-ICP-MS. Economic Geology, 2019, 114, 67-92.	3.8	26
35	Atmosphere oxygen cycling through the Proterozoic and Phanerozoic. Mineralium Deposita, 2019, 54, 485-506.	4.1	73
36	Elemental and B-O-H isotopic compositions of tourmaline and associated minerals in biotite-muscovite granite of Mashhad, NE Iran: Constraints on tourmaline genesis and element partitioning. Lithos, 2019, 324-325, 803-820.	1.4	13

LEONID V DANYUSHEVSKY

#	Article	IF	CITATIONS
37	Subduction initiation terranes exposed at the front of a 2 Ma volcanically-active subduction zone. Earth and Planetary Science Letters, 2019, 508, 30-40.	4.4	49
38	The trace (dispersed) elements in pyrite from the Fule Pb-Zn deposit, Yunnan Province, China, and its genetic information: A LA-ICPMS study. Acta Petrologica Sinica, 2019, 35, 3370-3384.	0.8	12
39	Role of upper-most crustal composition in the evolution of the Precambrian ocean–atmosphere system. Earth and Planetary Science Letters, 2018, 487, 44-53.	4.4	43
40	The Dovyren Intrusive Complex (Southern Siberia, Russia): Insights into dynamics of an open magma chamber with implications for parental magma origin, composition, and Cu-Ni-PGE fertility. Lithos, 2018, 302-303, 242-262.	1.4	28
41	Impact of air, laser pulse width and fluence on U–Pb dating of zircons by LA-ICPMS. Journal of Analytical Atomic Spectrometry, 2018, 33, 221-230.	3.0	84
42	The Boring Billion, a slingshot for Complex Life on Earth. Scientific Reports, 2018, 8, 4432.	3.3	63
43	Silicate-sulfide liquid immiscibility in modern arc basalt (Tolbachik volcano, Kamchatka): Part I. Occurrence and compositions of sulfide melts. Chemical Geology, 2018, 478, 102-111.	3.3	38
44	Immiscible sulfide melts in primitive oceanic magmas: Evidence and implications from picrite lavas (Eastern Kamchatka, Russia). American Mineralogist, 2018, 103, 886-898.	1.9	29
45	Genetic Interpretation of the Distribution of PGE and Chalcogens in Sulfide-Mineralized Ultramafic Rocks from the Yoko-Dovyren Layered Intrusion. Geochemistry International, 2018, 56, 1322-1340.	0.7	7
46	Geochemical evidence for the fractionation of iridium group elements at the early stages of crystallization of the Dovyren magmas (northern Baikal area, Russia). Russian Geology and Geophysics, 2018, 59, 459-471.	0.7	5
47	Sulfide Breccias from the Semenov-3 Hydrothermal Field, Mid-Atlantic Ridge: Authigenic Mineral Formation and Trace Element Pattern. Minerals (Basel, Switzerland), 2018, 8, 321.	2.0	12
48	Using integrated in-situ sulfide trace element geochemistry and sulfur isotopes to trace ore-forming fluids: Example from the Mina Justa IOCG deposit (southern Perú). Ore Geology Reviews, 2018, 101, 165-179.	2.7	36
49	Garnet-Pyroxenite-Derived End-Member Magma Type in Kamchatka: Evidence from Composition of Olivine and Olivine-Hosted Melt Inclusions in Holocene Rocks of Kekuknaisky Volcano. Petrology, 2018, 26, 329-350.	0.9	8
50	Seawater cycled throughout Earth's mantle in partially serpentinized lithosphere. Nature Geoscience, 2017, 10, 222-228.	12.9	139
51	Matrix dependency for oxide production rates by LA-ICP-MS. Journal of Analytical Atomic Spectrometry, 2017, 32, 638-646.	3.0	10
52	Covellite of the Semenov-2 hydrothermal field (13°31.13′ N, Mid-Atlantic Ridge): Enrichment in trace elements according to LA ICP MS analysis. Doklady Earth Sciences, 2017, 473, 291-295.	0.7	11
53	A triple S-shaped compositional profile in a Karoo dolerite sill—Evidence of concurrent multiple fractionation processes. Geology, 2017, 45, 603-606.	4.4	4
54	Criteria for the detection of hydrothermal ecosystem faunas in ores of massive sulfide deposits in the Urals. Lithology and Mineral Resources, 2017, 52, 173-191.	0.6	3

#	Article	IF	CITATIONS
55	Gold- and Silver-Rich Massive Sulfides from the Semenov-2 Hydrothermal Field, 13°31.13′N, Mid-Atlantic Ridge: A Case of Magmatic Contribution?. Economic Geology, 2017, 112, 741-773.	3.8	40
56	Ore fluid evolution in the giant Marcona Fe-(Cu) deposit, Perú: Evidence from in-situ sulfur isotope and trace element geochemistry of sulfides. Ore Geology Reviews, 2017, 86, 624-638.	2.7	16
57	Platinum-group elements and gold in sulfide melts from modern arc basalt (Tolbachik volcano,) Tj ETQq1 1 0.784	4314 rgBT 1.4	/Oyerlock 10
58	Se and In minerals in the submarine oxidation zone of a massive sulfide orebody of the molodezhnoe copper–zinc massive sulfide deposit, Southern Urals. Doklady Earth Sciences, 2017, 473, 318-322.	0.7	9
59	Tube fossils from gossanites of the Urals VHMS deposits, Russia: Authigenic mineral assemblages and trace element distributions. Ore Geology Reviews, 2017, 85, 107-130.	2.7	15
60	Chimneys in Paleozoic massive sulfide mounds of the Urals VMS deposits: Mineral and trace element comparison with modern black, grey, white and clear smokers. Ore Geology Reviews, 2017, 85, 64-106.	2.7	90
61	Cu–Ni–PGE fertility of the Yoko-Dovyren layered massif (northern Transbaikalia, Russia): thermodynamic modeling of sulfide compositions in low mineralized dunite based on quantitative sulfide mineralogy. Mineralium Deposita, 2016, 51, 993-1011.	4.1	29
62	Matrix effects in Pb/U measurements during LA-ICP-MS analysis of the mineral apatite. Journal of Analytical Atomic Spectrometry, 2016, 31, 1206-1215.	3.0	71
63	Pyrite compositions from VHMS and orogenic Au deposits in the Yilgarn Craton, Western Australia: Implications for gold and copper exploration. Ore Geology Reviews, 2016, 79, 474-499.	2.7	108
64	Textures, trace elements, and Pb isotopes of sulfides from the Haopinggou vein deposit, southern North China Craton: implications for discrete Au and Ag–Pb–Zn mineralization. Contributions To Mineralogy and Petrology, 2016, 171, 1.	3.1	49
65	Trace Element Content of Pyrite from the Kapai Slate, St. Ives Gold District, Western Australia. Economic Geology, 2016, 111, 1297-1320.	3.8	86
66	Abrupt transition from fractional crystallization to magma mixing at Gorely volcano (Kamchatka) after caldera collapse. Bulletin of Volcanology, 2016, 78, 1.	3.0	37
67	Evidence of Biogenic Activity in Quartz-Hematite Rocks of the Urals VMS Deposits. Lecture Notes in Earth System Sciences, 2016, , 109-122.	0.6	1
68	Relationships Between Gold and Pyrite at the Xincheng Gold Deposit, Jiaodong Peninsula, China: Implications for Gold Source and Deposition in a Brittle Epizonal Environment. Economic Geology, 2016, 111, 105-126.	3.8	202
69	Severe selenium depletion in the Phanerozoic oceans as a factor in three global mass extinction events. Gondwana Research, 2016, 36, 209-218.	6.0	44
70	Propagation of backâ€arc extension into the arc lithosphere in the southern <scp>N</scp> ew <scp>H</scp> ebrides volcanic arc. Geochemistry, Geophysics, Geosystems, 2015, 16, 3142-3159.	2.5	31
71	Synsedimentary to Early Diagenetic Gold in Black Shale-Hosted Pyrite Nodules at the Golden Mile Deposit, Kalgoorlie, Western Australia. Economic Geology, 2015, 110, 1157-1191.	3.8	70
72	Banded sulfide-magnetite ores of Mauk copper massive sulfide deposit, Central Urals: Composition and genesis. Geology of Ore Deposits, 2015, 57, 197-212.	0.7	8

#	Article	IF	CITATIONS
73	A model for carbonatite hosted REE mineralisation — the Mianning–Dechang REE belt, Western Sichuan Province, China. Ore Geology Reviews, 2015, 70, 595-612.	2.7	83
74	A laser ablation ICP-MS study of platinum-group and chalcophile elements in base metal sulfide minerals of the Jinchuan Ni–Cu sulfide deposit, NW China. Ore Geology Reviews, 2015, 65, 955-967.	2.7	41
75	Geology and genesis of the giant Beiya porphyry–skarn gold deposit, northwestern Yangtze Block, China. Ore Geology Reviews, 2015, 70, 457-485.	2.7	132
76	Trace Element Content of Sedimentary Pyrite in Black Shales. Economic Geology, 2015, 110, 1389-1410.	3.8	307
77	The Dovyren intrusive complex (<i>northern Baikal region, Russia</i>): isotope–geochemical markers of contamination of parental magmas and extreme enrichment of the source. Russian Geology and Geophysics, 2015, 56, 411-434.	0.7	29
78	Gold in the oceans through time. Earth and Planetary Science Letters, 2015, 428, 139-150.	4.4	72
79	Cycles of nutrient trace elements in the Phanerozoic ocean. Gondwana Research, 2015, 28, 1282-1293.	6.0	112
80	Barite-rich massive sulfides from the Semenov-1 hydrothermal field (Mid-Atlantic Ridge, 13°30.87′ N): Evidence for phase separation and magmatic input. Marine Geology, 2014, 349, 37-54.	2.1	54
81	Development and characterization of custom-engineered and compacted nanoparticles as calibration materials for quantification using LA-ICP-MS. Journal of Analytical Atomic Spectrometry, 2014, 29, 955-962.	3.0	31
82	Mineralogy and trace-element geochemistry of sulfide minerals in hydrothermal chimneys from the Upper-Cretaceous VMS deposits of the eastern Pontide orogenic belt (NE Turkey). Ore Geology Reviews, 2014, 63, 129-149.	2.7	126
83	Trace element content of sedimentary pyrite as a new proxy for deep-time ocean–atmosphere evolution. Earth and Planetary Science Letters, 2014, 389, 209-220.	4.4	384
84	Fractionation of sulphur relative to iron during laser ablation-ICP-MS analyses of sulphide minerals: implications for quantification. Journal of Analytical Atomic Spectrometry, 2014, 29, 1024-1033.	3.0	46
85	Optimisation of laser parameters for the analysis of sulphur isotopes in sulphide minerals by laser ablation ICP-MS. Journal of Analytical Atomic Spectrometry, 2014, 29, 1042-1051.	3.0	96
86	LA-ICP-MS trace element analysis of pyrite from the Chang'an gold deposit, Sanjiang region, China: Implication for ore-forming process. Gondwana Research, 2014, 26, 557-575.	6.0	176
87	Integrated stratigraphic–structural–hydrothermal alteration and mineralisation model for the Kangaroo Caves zinc–copper deposit, Western Australia. Australian Journal of Earth Sciences, 2014, 61, 159-185.	1.0	2
88	Subduction-related halogens (Cl, Br and I) and H2O in magmatic glasses from Southwest Pacific Backarc Basins. Earth and Planetary Science Letters, 2014, 400, 165-176.	4.4	52
89	High-grade iron ore at Windarling, Yilgarn Craton: a product of syn-orogenic deformation, hypogene hydrothermal alteration and supergene modification in an Archean BIF-basalt lithostratigraphy. Mineralium Deposita, 2013, 48, 697-728.	4.1	38
90	Geochronology of the Dovyren intrusive complex, northwestern Baikal area, Russia, in the Neoproterozoic. Geochemistry International, 2013, 51, 859-875.	0.7	52

#	Article	IF	CITATIONS
91	Evidence for an Intrabasinal Source and Multiple Concentration Processes in the Formation of the Carbon Leader Reef, Witwatersrand Supergroup, South Africa. Economic Geology, 2013, 108, 1215-1241.	3.8	63
92	A Comparative Study of Five Reference Materials and the Lombard Meteorite for the Determination of the Platinumâ€Group Elements and Gold by LAâ€ICPâ€MS. Geostandards and Geoanalytical Research, 2013, 37, 51-64.	3.1	53
93	Tellurium-bearing minerals in zoned sulfide chimneys from Cu-Zn massive sulfide deposits of the Urals, Russia. Mineralogy and Petrology, 2013, 107, 67-99.	1.1	38
94	Trace element heterogeneity in molybdenite fingerprints stages of mineralization. Chemical Geology, 2013, 347, 175-189.	3.3	62
95	Modeling Solubility of Fe-Ni Sulfides in Basaltic Magmas: The Effect of Nickel. Economic Geology, 2013, 108, 1983-2003.	3.8	69
96	Geochemical Evolution of the Banded Iron Formation-Hosted High-Grade Iron Ore System in the Koolyanobbing Greenstone Belt, Western Australia. Economic Geology, 2012, 107, 599-644.	3.8	71
97	Partitioning of elements between silicate melt and immiscible fluoride, chloride, carbonate, phosphate and sulfate melts, with implications to the origin of natrocarbonatite. Geochimica Et Cosmochimica Acta, 2012, 79, 20-40.	3.9	177
98	Ferruginous and manganiferous haloes around massive sulphide deposits of the Urals. Ore Geology Reviews, 2012, 47, 5-41.	2.7	39
99	Structural, lithological, and geochemical constraints on the dynamic magma plumbing system of the Jinchuan Ni–Cu sulfide deposit, NW China. Mineralium Deposita, 2012, 47, 277-297.	4.1	69
100	Routine quantitative multi-element analysis of sulphide minerals by laser ablation ICP-MS: Standard development and consideration of matrix effects. Geochemistry: Exploration, Environment, Analysis, 2011, 11, 51-60.	0.9	211
101	The effect of quadrupole ICPMS interface and ion lens design on argide formation. Implications for LA-ICPMS analysis of PGE's in geological samples. Journal of Analytical Atomic Spectrometry, 2011, 26, 1401.	3.0	34
102	The effect of silica contents on Pd, Pt and Rh solubilities in silicate melts: an experimental study. European Journal of Mineralogy, 2011, 23, 355-367.	1.3	50
103	Indium mineralisation in A-type granites in southeastern Finland: Insights into mineralogy and partitioning between coexisting minerals. Chemical Geology, 2011, 284, 62-73.	3.3	76
104	Melt inclusion Pb-isotope analysis by LA–MC-ICPMS: Assessment of analytical performance and application to OIB genesis. Chemical Geology, 2011, 289, 210-223.	3.3	39
105	Minor and trace elements in bornite and associated Cu–(Fe)-sulfides: A LA-ICP-MS studyBornite mineral chemistry. Geochimica Et Cosmochimica Acta, 2011, 75, 6473-6496.	3.9	118
106	Petrolog3: Integrated software for modeling crystallization processes. Geochemistry, Geophysics, Geosystems, 2011, 12, n/a-n/a.	2.5	431
107	Trace and minor elements in sphalerite from base metal deposits in South China: A LA-ICPMS study. Ore Geology Reviews, 2011, 39, 188-217.	2.7	327
108	In memoriam Vyacheslav Ivanovich Kovalenko. Petrology, 2011, 19, 325-326.	0.9	0

#	Article	IF	CITATIONS
109	Volatile Evolution of Magma Associated with the Solchiaro Eruption in the Phlegrean Volcanic District (Italy). Journal of Petrology, 2011, 52, 2431-2460.	2.8	68
110	Elemental fingerprints of southern calamary (<i>Sepioteuthis australis</i>) reveal local recruitment sources and allow assessment of the importance of closed areas. Canadian Journal of Fisheries and Aquatic Sciences, 2011, 68, 1351-1360.	1.4	18
111	Geochemical characteristics and Sr–Nd–Hf isotope compositions of mantle xenoliths and host basalts from Assab, Eritrea: implications for the composition and thermal structure of the lithosphere beneath the Afar Depression. Contributions To Mineralogy and Petrology, 2010, 159, 731-751.	3.1	32
112	Transgenerational marking of cephalopods with an enriched barium isotope: a promising tool for empirically estimating post-hatching movement and population connectivity. ICES Journal of Marine Science, 2010, 67, 1372-1380.	2.5	10
113	The Dovyren intrusive complex: Problems of petrology and Ni sulfide mineralization. Geochemistry International, 2009, 47, 425-453.	0.7	25
114	Otolith chemistry reveals fine population structure and close affinity to the Pacific and Atlantic oceanic spawning grounds in the migratory southern blue whiting (Micromesistius australis) Tj ETQq0 0 0 rgBT /0	Dv ert ock 1	0 4650 537
115	In situ Pb-isotope analysis of pyrite by laser ablation (multi-collector and quadrupole) ICPMS. Chemical Geology, 2009, 262, 344-354.	3.3	74
116	â€~Invisible gold' in bismuth chalcogenides. Geochimica Et Cosmochimica Acta, 2009, 73, 1970-1999.	3.9	106
117	Trace and minor elements in sphalerite: A LA-ICPMS study. Geochimica Et Cosmochimica Acta, 2009, 73, 4761-4791.	3.9	581
118	Primitive shoshonites from Fiji: Geochemistry and source components. Geochemistry, Geophysics, Geosystems, 2009, 10, .	2.5	44
119	Gold and Trace Element Zonation in Pyrite Using a Laser Imaging Technique: Implications for the Timing of Gold in Orogenic and Carlin-Style Sediment-Hosted Deposits. Economic Geology, 2009, 104, 635-668.	3.8	748
120	Study of Trace Element Zonation in Vent Chimneys from the Silurian Yaman-Kasy Volcanic-Hosted Massive Sulfide Deposit (Southern Urals, Russia) Using Laser Ablation-Inductively Coupled Plasma Mass Spectrometry (LA-ICPMS). Economic Geology, 2009, 104, 1111-1141.	3.8	267
121	Geochemical and isotopic signatures of magmatic products in the MAR rift valley at 12°49′–17°23′ N 29°59′–33°41′ N: Evidence of Two contrasting sources of the parental melts. Petrology, 2008, 16, 36-	and 62.9	7
122	Oxidation state of iron in komatiitic melt inclusions indicates hot Archaean mantle. Nature, 2008, 455, 960-963.	27.8	180
123	Age and pyrite Pb-isotopic composition of the giant Sukhoi Log sediment-hosted gold deposit, Russia. Geochimica Et Cosmochimica Acta, 2008, 72, 2377-2391.	3.9	151
124	High-Mg adakites from Kadavu Island Group, Fiji, southwest Pacific: Evidence for the mantle origin of adakite parental melts. Geology, 2008, 36, 499.	4.4	55
125	The Composition of Near-solidus Partial Melts of Fertile Peridotite at 1 and 1·5 GPa: Implications for the Petrogenesis of MORB. Journal of Petrology, 2008, 49, 591-613.	2.8	78
126	Using stylet elemental signatures to determine the population structure of Octopus maorum. Marine Ecology - Progress Series, 2008, 360, 125-133.	1.9	15

LEONID V DANYUSHEVSKY

#	Article	IF	CITATIONS
127	Stylet elemental signatures indicate population structure in a holobenthic octopus species, Octopus pallidus. Marine Ecology - Progress Series, 2008, 371, 1-10.	1.9	17
128	Multistage Sedimentary and Metamorphic Origin of Pyrite and Gold in the Giant Sukhoi Log Deposit, Lena Gold Province, Russia. Economic Geology, 2007, 102, 1233-1267.	3.8	457
129	Boninites and Adakites from the Northern Termination of the Tonga Trench: Implications for Adakite Petrogenesis. Journal of Petrology, 2007, 49, 697-715.	2.8	137
130	The application of olivine geothermometry to infer crystallization temperatures of parental liquids: Implications for the temperature of MORB magmas. Chemical Geology, 2007, 241, 207-233.	3.3	77
131	Multiple mantle plume components involved in the petrogenesis of subductionâ€related lavas from the northern termination of the Tonga Arc and northern Lau Basin: Evidence from the geochemistry of arc and backarc submarine volcanics. Geochemistry, Geophysics, Geosystems, 2007, 8, .	2.5	105
132	The amount of recycled crust in sources of mantle-derived melts. Science, 2007, 316, 412-7.	12.6	822
133	The Amount of Recycled Crust in Sources of Mantle-Derived Melts. Science, 2007, 316, 412-417.	12.6	470
134	Crystallization temperatures of tholeiite parental liquids: Implications for the existence of thermally driven mantle plumes. , 2007, , 235-260.		14
135	MPI-DING reference glasses for in situ microanalysis: New reference values for element concentrations and isotope ratios. Geochemistry, Geophysics, Geosystems, 2006, 7, n/a-n/a.	2.5	563
136	Immiscible silicate liquid partition coefficients: implications for crystal-melt element partitioning and basalt petrogenesis. Contributions To Mineralogy and Petrology, 2006, 152, 685-702.	3.1	109
137	Petrogenetic variability along the North?South Propagating Spreading Center of the North Fiji Basin. Mineralogy and Petrology, 2005, 83, 55-86.	1.1	7
138	Metals in quartz-hosted melt inclusions: Natural facts and experimental artifacts. American Mineralogist, 2005, 90, 1674-1678.	1.9	34
139	Major element and primary sulfur concentrations in Apollo 12 mare basalts: The view from melt inclusions. Meteoritics and Planetary Science, 2005, 40, 679-693.	1.6	30
140	Oxygen isotope evidence for slab melting in modern and ancient subduction zones. Earth and Planetary Science Letters, 2005, 235, 480-496.	4.4	217
141	Kimberlite melts rich in alkali chlorides and carbonates: A potent metasomatic agent in the mantle. Geology, 2004, 32, 845.	4.4	229
142	Melt Inclusions in Primitive Olivine Phenocrysts: the Role of Localized Reaction Processes in the Origin of Anomalous Compositions. Journal of Petrology, 2004, 45, 2531-2553.	2.8	136
143	Crustal origin for coupled 'ultra-depleted' and 'plagioclase' signatures in MORB olivine-hosted melt inclusions: evidence from the Siqueiros Transform Fault, East Pacific Rise. Contributions To Mineralogy and Petrology, 2003, 144, 619-637.	3.1	86
144	A model for the evolution of the Mt. Somma-Vesuvius magmatic system based on fluid and melt inclusion investigations. Developments in Volcanology, 2003, 5, 227-249.	0.5	22

#	Article	IF	CITATIONS
145	Plate-kinematic explanation for mid-oceanic-ridge depth discontinuities. Geology, 2003, 31, 399.	4.4	28
146	Melt Inclusions in Olivine Phenocrysts: Using Diffusive Re-equilibration to Determine the Cooling History of a Crystal, with Implications for the Origin of Olivine-phyric Volcanic Rocks. Journal of Petrology, 2002, 43, 1651-1671.	2.8	136
147	Experimental and petrological studies of melt inclusions in phenocrysts from mantle-derived magmas: an overview of techniques, advantages and complications. Chemical Geology, 2002, 183, 5-24.	3.3	372
148	Relationships between Campi Flegrei and Mt. Somma volcanism: evidence from melt inclusions in clinopyroxene phenocrysts from volcanic breccia xenoliths. Mineralogy and Petrology, 2001, 73, 107-119.	1.1	14
149	The effect of small amounts of H2O on crystallisation of mid-ocean ridge and backarc basin magmas. Journal of Volcanology and Geothermal Research, 2001, 110, 265-280.	2.1	294
150	Peridotite Melting at 1 GPa: Reversal Experiments on Partial Melt Compositions Produced by Peridotite-Basalt Sandwich Experiments. Journal of Petrology, 2001, 42, 2363-2390.	2.8	80
151	Re-equilibration of melt inclusions trapped by magnesian olivine phenocrysts from subduction-related magmas: petrological implications. Contributions To Mineralogy and Petrology, 2000, 138, 68-83.	3.1	384
152	Melting of Refractory Mantle at 1middle dot5, 2 and 2middle dot5 GPa under Anhydrous and H2O-undersaturated Conditions: Implications for the Petrogenesis of High-Ca Boninites and the Influence of Subduction Components on Mantle Melting. Journal of Petrology, 2000, 41, 257-283.	2.8	326
153	H2O Abundance in Depleted to Moderately Enriched Mid-ocean Ridge Magmas; Part I: Incompatible Behaviour, Implications for Mantle Storage, and Origin of Regional Variations. Journal of Petrology, 2000, 41, 1329-1364.	2.8	167
154	Peridotite Melting at 1.0 and 1.5 GPa: an Experimental Evaluation of Techniques using Diamond Aggregates and Mineral Mixes for Determination of Near-solidus Melts. Journal of Petrology, 1999, 40, 1343-1375.	2.8	133
155	Extensive volcaniclastic deposits at the Mid-Atlantic Ridge axis: results of deep-water basaltic explosive volcanic activity?. Terra Nova, 1998, 10, 280-286.	2.1	59
156	Coexistence of two distinct mantle sources during formation of ophiolites: a case study of primitive pillow-lavas from the lowest part of the volcanic section of the Troodos Ophiolite, Cyprus. Contributions To Mineralogy and Petrology, 1997, 128, 287-301.	3.1	56
157	Direct oxygen measurements of Cr-rich spinel; implications for spinel stoichiometry. American Mineralogist, 1996, 81, 1186-1194.	1.9	10
158	Estimation of the pressure of crystallization and H2O content of MORB and BABB glasses: calibration of an empirical technique. Mineralogy and Petrology, 1996, 57, 185-204.	1.1	53
159	Ferric-ferrous ratio and oxygen fugacity calculations for primitive mantle-derived melts: calibration of an empirical technique. Mineralogy and Petrology, 1996, 57, 229-241.	1.1	31
160	An experimental study of the effects of melt composition on plagioclase-melt equilibria at 5 and 10 kbar: implications for the origin of magmatic high-An plagioclase. Contributions To Mineralogy and Petrology, 1995, 118, 420-432.	3.1	251
161	North Tongan high-Ca boninite petrogenesis: The role of samoan plume and subduction zone-transform fault transition. Journal of Geodynamics, 1995, 20, 219-241.	1.6	78
162	Petrology and Geochemistry of Boninites from the North Termination of the Tonga Trench: Constraints on the Generation Conditions of Primary High-Ca Boninite Magmas. Journal of Petrology, 1994, 35, 1183-1211.	2.8	316

#	Article	IF	CITATIONS
163	High-Mg andesites from the southern termination of the New Hebrides island arc (SW Pacific). Journal of Volcanology and Geothermal Research, 1993, 57, 193-217.	2.1	62
164	The H2O content of basalt glasses from Southwest Pacific back-arc basins. Earth and Planetary Science Letters, 1993, 117, 347-362.	4.4	132
165	Melting History of an Ultrahigh-pressure Paragneiss Revealed by Multiphase Solid Inclusions in Garnet, Kokchetav Massif, Kazakhstan. Journal of Petrology, 0, , egw049.	2.8	16